Higher-order many-body perturbation-theory calculations of energy levels in cesium

S. A. Blundell, W. R. Johnson, and J. Sapirstein
Department of Physics, University of Notre Dame, Notre Dame, Indiana 46556
and Institute for Theoretical Physics, University of California, Santa Barbara, California 93106
(Received 10 June 1988)

The question of which contributions to the energy levels of cesium must be included in many-body perturbation theory to achieve accuracies of parts per thousand is addressed. To this end, we evaluate second- and third-order correlation corrections to the energy levels of several states. When these corrections are supplemented with two dominant classes of corrections from fourth and higher order, the calculated energy of each of the states considered is brought to within a few parts per thousand of the measured energy. Implications for calculations of transition amplitudes, in particular, amplitudes of parity-nonconserving transitions, are discussed.

Because of recent high-accuracy measurements of parity-nonconserving (PNC) amplitudes in cesium, the general question of the ability of atomic theory to account for the structure of this atom at the few-percent level of accuracy has become of particular interest. The present error in the measurement for the $6s \rightarrow 7s$ PNC dipole amplitude in cesium is 2.5%, and this error can be reduced to under 1%.[1] The study of PNC in cesium yields valuable information about the structure of unified theories of the weak and electromagnetic interactions,[2] so it is clearly of interest to identify methods capable of predicting properties of cesium with high accuracy. While a variety of techniques can be employed to study atomic structure, a particularly powerful and systematic approach is afforded by relativistic many-body perturbation theory (MBPT). A recent application of MBPT to energy levels and parity-conserving transitions in cesium and in lighter alkali atoms has been given in Ref. 3, and the extension to PNC transitions is given in Ref. 4. Briefly, the conclusions of Ref. 3 were that MBPT calculations carried out through second order for energies and third order for matrix elements differed from experiment at the 1% level for the former, and by up to 5% for the latter. Since the ultimate goal of these calculations is to achieve accuracies well under 1%, it is clear that higher orders in perturbation theory must be considered. However, because the order-by-order implementation of MBPT becomes computationally unwieldy beyond third order, it is vital to identify dominant classes of terms, and when necessary to sum particular classes of corrections to infinite order. It is the purpose of this paper to report our experience with the behavior of MBPT for the calculation of valence electron ionization energies in cesium. We have found, starting from a V^{N-1} Hartree-Fock model, that although the inclusion of second-order MBPT corrections provides dramatic improvement of the lowest-order energies, reducing the error from roughly 10% to 1%, the third-order correction fails to give any further improvement. An iteration of the large second-order effect allows us to sum an infinite class of fourth- and higher-order MBPT terms. The inclusion of these terms together with another class of fourth-order terms related to the second-order energy correction leads to a dramatic improvement of the energies to within a few tenths of a percent of the measured values. A detailed description of the large-scale third-order computation will be presented along with a description of the iterative scheme used to determine the higher-order corrections. We will discuss the results and their possible implications for transition amplitude calculations.

The third-order MBPT formulas for valence electron removal energies in one-valence electron atoms are represented by the graphs of Figs. 1(a)–1(l). Additional graphs which we would have to consider if we were not starting our calculation from a V^{N-1} potential are not

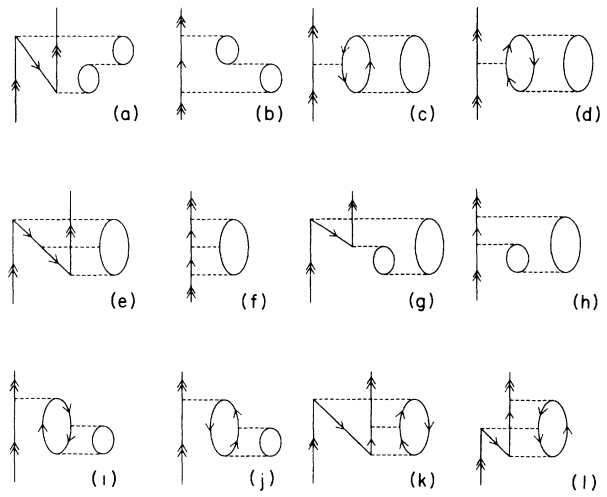

FIG. 1. Brueckner-Goldstone graphs contributing to the third-order energy. Exchange variants are suppressed, as are the complex-conjugate graphs in (g)–(l).

shown. The explicit expressions for the graphs of Figs. 1(a)–1(l) are as follows:

$$E_A^{(3)} = -\frac{\tilde{g}_{canv}\tilde{g}_{mvba}\tilde{g}_{nbcm}}{(\varepsilon_{ac}-\varepsilon_{nv})(\varepsilon_{ab}-\varepsilon_{vm})}\ , \tag{1a}$$

$$E_B^{(3)} = \frac{\tilde{g}_{vbmr}\tilde{g}_{mnva}\tilde{g}_{rabn}}{(\varepsilon_{av}-\varepsilon_{mn})(\varepsilon_{bv}-\varepsilon_{rm})}\ , \tag{1b}$$

$$E_C^{(3)} = -\frac{\tilde{g}_{acmn}g_{mnab}\tilde{g}_{vbvc}}{(\varepsilon_{ac}-\varepsilon_{mn})(\varepsilon_{ab}-\varepsilon_{mn})}\ , \tag{1c}$$

$$E_D^{(3)} = \frac{\tilde{g}_{abrn}g_{mnab}\tilde{g}_{vrvm}}{(\varepsilon_{ab}-\varepsilon_{rn})(\varepsilon_{ab}-\varepsilon_{mn})}\ , \tag{1d}$$

$$E_E^{(3)} = -\frac{\tilde{g}_{cdmv}g_{mvab}g_{abcd}}{(\varepsilon_{ab}-\varepsilon_{vm})(\varepsilon_{cd}-\varepsilon_{vm})}\ , \tag{1e}$$

$$E_F^{(3)} = \frac{\tilde{g}_{avsr}g_{mnav}g_{rsnm}}{(\varepsilon_{av}-\varepsilon_{mn})(\varepsilon_{av}-\varepsilon_{rs})}\ , \tag{1f}$$

$$E_G^{(3)} = -\frac{\tilde{g}_{nmac}\tilde{g}_{abnv}\tilde{g}_{vcbm}}{(\varepsilon_{ab}-\varepsilon_{vn})(\varepsilon_{ac}-\varepsilon_{mn})} + \text{c.c.}\ , \tag{1g}$$

$$E_H^{(3)} = \frac{\tilde{g}_{mrab}\tilde{g}_{avmn}\tilde{g}_{nbvr}}{(\varepsilon_{av}-\varepsilon_{mn})(\varepsilon_{ab}-\varepsilon_{rm})} + \text{c.c.}\ , \tag{1h}$$

$$E_I^{(3)} = -\frac{\tilde{g}_{mncb}\tilde{g}_{vavm}g_{cban}}{(\varepsilon_{a}-\varepsilon_{m})(\varepsilon_{cb}-\varepsilon_{mn})} + \text{c.c.}\ , \tag{1i}$$

$$E_J^{(3)} = \frac{\tilde{g}_{rnab}\tilde{g}_{vavm}g_{bmnr}}{(\varepsilon_{a}-\varepsilon_{m})(\varepsilon_{ab}-\varepsilon_{nr})} + \text{c.c.}\ , \tag{1j}$$

$$E_K^{(3)} = -\frac{\tilde{g}_{mnab}g_{abrv}g_{rvmn}}{(\varepsilon_{ab}-\varepsilon_{vr})(\varepsilon_{ab}-\varepsilon_{mn})} + \text{c.c.}\ , \tag{1k}$$

$$E_L^{(3)} = \frac{\tilde{g}_{mncb}g_{avmn}g_{bcva}}{(\varepsilon_{av}-\varepsilon_{mn})(\varepsilon_{bc}-\varepsilon_{mn})} + \text{c.c.} \tag{1l}$$

Several conventions are assumed in the above formulas. All core indices (a, b, c and d) and all excited state indices (m, n, r, and s) are implicitly summed over; v denotes the valence state. The symbol ε_{xy} denotes a sum of single-particle energies $\varepsilon_x+\varepsilon_y$, and $\tilde{g}_{wxyz}\equiv g_{wxyz}-g_{wxzy}$, where g_{abcd} is the Coulomb matrix element,

$$g_{abcd} \equiv \int \frac{d\mathbf{x}\,d\mathbf{y}}{|\mathbf{x}-\mathbf{y}|}\psi_a^\dagger(\mathbf{x})\psi_c(\mathbf{x})\psi_b^\dagger(\mathbf{y})\psi_d(\mathbf{y})\ . \tag{2}$$

Note that only one graph is shown for each term in Eqs. (1a)–(1l), corresponding to $\tilde{g}_{abcd}\rightarrow g_{abcd}$; it should be emphasized that each graph has either one, three, or seven partners that are not explicitly shown, though they are evaluated in the following calculations. Finally, the notation c.c. refers to addition of complex-conjugate terms, which are obtained graphically by reflecting Figs. 1(g)–1(l) about a horizontal axis, but give the same contribution.

Because at this stage we are implementing MBPT in an order-by-order manner, as opposed to using so-called *all-orders* methods,[5] the role of our third-order energy calculation in the all-orders framework will now be discussed. All-orders methods are methods that sum important classes of diagrams built up iteratively from low-order diagrams. In higher order there are generally terms that will be missed by any given all-orders scheme; such terms can be evaluated individually. For one-valence electron atoms, a powerful and accurate all-orders method that can sum all terms associated with both single and double excitations of core electrons is the coupled-cluster method. The coupled-cluster method has been applied to neutral lithium to obtain highly accurate energies by Lindgren.[6] This particular method picks up the graphs 1(a), 1(b), 1(e), and 1(f), but omits graphs 1(c) and 1(d) entirely. In addition, in the standard implementation, the graphs 1(g)–1(l) are also included, but the corresponding c.c. graphs are omitted. It is, however, possible to modify the coupled-cluster method to include both these c.c. terms and graphs 1(c) and 1(d).[7] In the following we tabulate the third-order graphs individually, so that our results can be combined with the coupled-cluster methods if desired.

We have discussed the evaluation of third-order graphs in considerable detail elsewhere.[8] However, our previous work was carried out on the light alkalis, and cesium presents considerably greater numerical challenges, forcing us to make certain approximations. Our experience with the second-order energy shows that the deep core states of cesium play a very small role in determining the corrections to valence energies. For this reason, we left the shells with principal quantum numbers $n=1$, 2, and 3 inert in the present third-order calculation, and allowed the core summations to range over the $4s_{1/2}$, $4p_{1/2}$, $4p_{3/2}$, $4d_{3/2}$, $4d_{5/2}$, $5s_{1/2}$, $5p_{1/2}$, and $5p_{3/2}$ core states only; when this same restriction is applies to the second-order energy it changes the value by less than 1%. Since our calculation is carried out using finite basis set techniques, the amount of computing required is strongly dependent on the size of the basis set: if we were to use the same basis set that we employed in our second-order calculation, which consisted of 40 states for each κ value, we would not have been able to carry out the third-order calculation with the computing resources available to us. Two devices permitted us to overcome this difficulty. While the size n of the basis set was left relatively large ($n=32$) for s, p, and d states (which dominate the calculation), for states of higher angular momentum a smaller basis set ($n=16$) was used.[9] The next approximation relied on the fact that those states in our basis set which represent high-energy continuum states lead to extremely large energy denominators and relatively small overlap integrals in the numerators of the MBPT formulas; these terms therefore play a negligible role. This is particularly true of the s, p, and d states, for which about one-half of the spectrum could be neglected; for $l>2$ this was less true, so no truncation was made there. Thus the basis set was effectively reduced to a manageable size of $n=16$. The error introduced by these approximations in the second-order energy and in certain third-order corrections was tested and was found to be less than 1%. The final approximation made was to restrict the number of partial waves summed to five, instead of retaining the

nine or ten used in the second-order calculation. We estimate that the net effect of all the approximations used introduces an error of less than 3% in $E^{(3)}$ for s states and 6% for p states.

In this paper we also consider two classes of higher-order corrections. Both of these corrections are expected to be important, since they are related to iterations of the large second-order energy diagrams. The dominant part of the second-order term comes from the expression

$$E^{(2)}_{\text{double}}=\frac{g_{mnva}\tilde{g}_{vamn}}{\varepsilon_{av}-\varepsilon_{mn}} . \tag{3}$$

This expression can also, however, be thought of as the first term in the following iterative scheme, which is a form of the Bethe-Salpeter equation:

$$E^{(2\cdots n)}=\tilde{g}_{vamn}\rho^{[n-1]}_{mnva} , \tag{4a}$$

$$\rho^{[n+1]}_{mnva}\equiv\frac{g_{mnva}}{\varepsilon_{av}-\varepsilon_{mn}}+\frac{g_{mnrs}\rho^{[n]}_{rsva}}{\varepsilon_{av}-\varepsilon_{mn}} . \tag{4b}$$

It is straightforward to see that $E^{(3)}_F$ results from the first iteration; because of its large contribution, it is clear that higher-order terms will play a significant role. For this reason we choose to evaluate the next iteration,

$$E^{(4)}_A=\frac{g_{mnxy}g_{xyrs}g_{rsva}\tilde{g}_{vamn}}{(\varepsilon_{av}-\varepsilon_{mn})(\varepsilon_{av}-\varepsilon_{xy})(\varepsilon_{av}-\varepsilon_{rs})} , \tag{5}$$

which is represented in Fig. 2; when viewed together with the second-order energy and the part of the third-order energy associated with Fig. 1(f), it is seen that we are evaluating ladder graphs with two, three, and four rungs. The sum to all orders of this set of ladder graphs is of central importance in nuclear physics, because of the strong repulsive short-range forces between nucleons. For the present calculation, however, this partial series converges rapidly: for example, for the 6s energy in cesium the contributions from $E^{(2)}$, $E^{(3)}_F$, and $E^{(4)}_A$ are, respectively, $-0.019\,26$, $+0.0050$, and -0.0010 a.u. Note

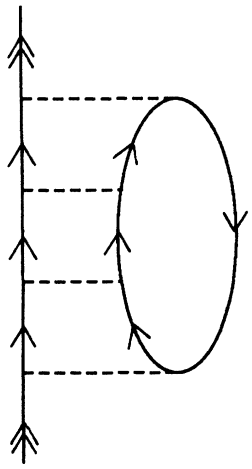

FIG. 2. Brueckner-Goldstone graph for $E^{(4)}_A$, defined in Eq. (5).

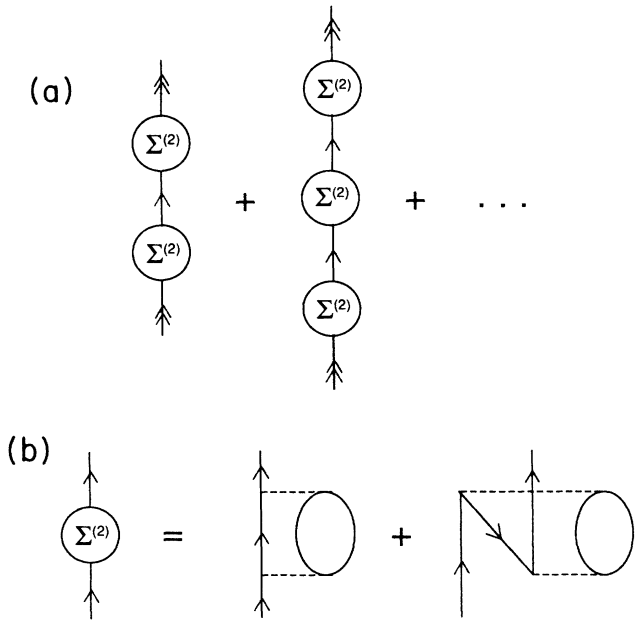

FIG. 3. (a) Iterated Brueckner (IBR) graphs formed by chaining the second-order self-energies. (b) Graphical definition of $\Sigma^{(2)}(\varepsilon)$, defined in Eq. (6).

the alternation in signs of this series, which follows from the fact that $\varepsilon_{av}-\varepsilon_{mn}$ is a negative quantity. Although we terminate the iteration at fourth order, it is possible to sum this series to convergence. We plan to continue the iteration in the framework of the much more complete (and computationally demanding) coupled-cluster approach; work on this is now in progress.

The second set of fourth- and higher-order graphs included in the present calculation is shown in Fig. 3. In our scheme, we sum chains of second-order *self-energy* units, which are defined by the relation

$$\langle i\,|\,\Sigma^{(2)}(\varepsilon)\,|\,j\rangle\equiv\Sigma^{(2)}_{ij}(\varepsilon)=\frac{g_{aimn}\tilde{g}_{mnaj}}{\varepsilon_a+\varepsilon-\varepsilon_{mn}}-\frac{g_{abjm}\tilde{g}_{imab}}{\varepsilon_{ab}-\varepsilon_m-\varepsilon} , \tag{6}$$

where i and j are arbitrary states, and where the core state a, and the excited states m and n, are summed over implicitly. With this definition, the second-order valence ionization energy for a valence state v is the diagonal matrix element of the self-energy operator:

$$E^{(2)}=\langle v\,|\,\Sigma^{(2)}(\varepsilon_v)\,|\,v\rangle . \tag{7}$$

The chaining of the self-energy units is achieved by solving iteratively the following set of equations:

$$\delta\varepsilon^{[n+1]}_v=\Sigma^{(2)}_{vv}(\varepsilon_v)+\Sigma^{(2)}_{vj}(\varepsilon_v)\rho^{[n]}_{jv} , \tag{8a}$$

$$(\varepsilon_v+\delta\varepsilon^{[n]}_v-\varepsilon_i)\rho^{[n]}_{iv}=\Sigma^{(2)}_{iv}(\varepsilon_v)+\Sigma^{(2)}_{ij}(\varepsilon_v)\rho^{[n-1]}_{jv} . \tag{8b}$$

Thus $\delta\varepsilon^{[1]}_v$ is equal to the second-order energy. On iteration, one generates the subset of fourth- and higher-order

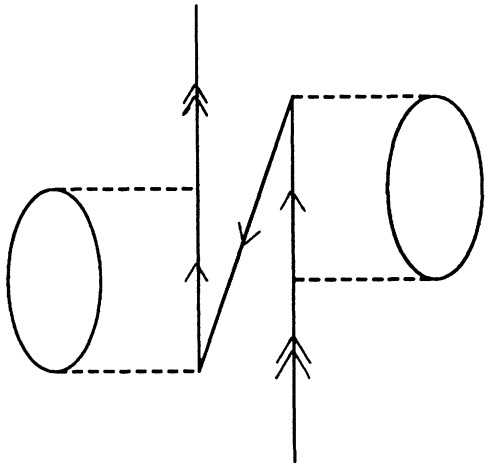

FIG. 4. Example of two self-energies connected by a core line. This is one of five possible time orderings.

terms depicted in Fig. 3. Note that the sum over states in the lines connecting the self-energy units in Fig. 3 can include both core and excited states (but must exclude the valence state v); correspondingly, i and j in Eq. (8b) refer to all states, both core and excited. An example of a MBPT diagram arising from a connection on a core line is given in Fig. 4. Finally, the $\delta\varepsilon_v^{[n]}$ in Eq. (8b) generate a subset of so-called *folded* diagrams starting in sixth order.

For this second class of corrections we have iterated the equation until convergence. The fourth-order contribution for the $6s$ state was -0.0024 a.u.; after convergence, this result changed to -0.0027 a.u., making it clear that there are significant contributions at the tenth of a percent level from diagrams of order six and above.

The lowest order v^{N-1} Hartree-Fock and second-order energy corrections have been discussed previously,[3] and we simply present them in the first two rows of Table I for the three states considered here, namely, the $6s_{1/2}$, $6p_{1/2}$, and $7s_{1/2}$ states. In the third row the third-order energy is given. It is of interest to consider the breakdown of the complicated expression for the third-order energy, so in Table II the contributions of $E_A^{(3)}-E_L^{(3)}$ are shown. Note that we combine Figs. 1(c) and 1(d), and Figs. 1(j) and 1(k). These graphs, which differ only by the direction indicated in the closed loop, are individually quite large, but almost precisely cancel. In the next row we give $E_A^{(4)}$. A feature of this class of diagram is that for higher partial waves, the number of allowed channels grows rapidly. This growth is particularly rapid in relativistic calculations because of the existence of two κ values for each value of l. For this reason we were forced to consider only three partial waves, truncating at $l=2$. In addition, only the dominant $5p_{3/2}$ and $5p_{1/2}$ core states were included. While this procedure for second- and third-order calculations is good in 10%, we assign a larger error of 20% to be conservative. In the fifth row of the table we list the values of the iterated Brueckner corrections $E_{\rm IBR}^{(4\cdots)}$ defined by

$$E_{\rm IBR}^{(4\cdots)}=\delta\varepsilon_v^{[2]}+\delta\varepsilon_v^{[3]}+\cdots . \tag{9}$$

In the final two rows of the table, the sum of the theoretical contributions is compared to the experimental energy.

Perhaps the most striking result of this calculation is the size of the contributions of third and higher order. While the end result is in agreement with experiment at the few tenths of a percent level, which is also the size of our numerical uncertainties, this agreement arises from cancellations of contributions of several percent. For example, the $6s_{1/2}$ energy differs from experiment by $+1.4\%$ in magnitude after including the second-order correction. However, if one then includes only the third-order correction, the theoretical value would differ from experiment by -2.8%, a significantly less accurate result. Only after the inclusion of the selected set of fourth- and higher-order terms described above does the situation improve. While it would be desirable to have a more smoothly convergent perturbation expansion, it is a

TABLE II. Decomposition of $E^{(3)}$ (atomic units).

State	$6s_{1/2}$	$6p_{1/2}$	$7s_{1/2}$
$E_A^{(3)}$	0.000 24	0.000 10	0.000 06
$E_B^{(3)}$	−0.004 68	−0.001 89	−0.001 10
$E_{C+D}^{(3)}$	−0.000 14	−0.000 20	−0.000 04
$E_E^{(3)}$	−0.000 21	−0.000 11	−0.000 05
$E_F^{(3)}$	0.004 95	0.001 82	0.001 20
$E_G^{(3)}$	0.000 40	0.000 11	0.000 10
$E_H^{(3)}$	0.004 34	0.001 69	0.001 04
$E_{I+J}^{(3)}$	0.000 85	0.000 21	0.000 21
$E_K^{(3)}$	−0.000 43	−0.000 21	−0.000 11
$E_L^{(3)}$	0.000 31	0.000 11	0.000 08

TABLE I. MBPT contributions to valence energies of cesium (atomic units).

State	$6s_{1/2}$	$6p_{1/2}$	$7s_{1/2}$
$E_{\rm HF}$	−0.127 37	−0.085 62	−0.055 19
$E^{(2)}$	−0.017 74	−0.006 91	−0.004 20
$E^{(3)}$	0.005 63(17)	0.001 63(10)	0.001 39(4)
$E_A^{(4)}$	−0.001 01(20)	−0.000 38(8)	−0.000 25(5)
$E_{\rm IBR}^{(4\cdots)}$	−0.002 69(3)	−0.001 10(3)	−0.000 19
$E_{\rm total}$	−0.143 18(26)	−0.092 38(13)	−0.058 44(6)
$E_{\rm expt}$	−0.143 10	−0.092 17	−0.058 65

well-known feature of the many-body problem that a more natural expansion is one in terms of the number of excited core electrons.[5] The full implementation of a relativistic version of one of these schemes for a system the size of cesium is an extremely-large-scale task. The role of the present calculation in this framework is as follows. By including $E^{(2)}$, $E_F^{(3)}$, $E_A^{(4)}$, and $E_{\mathrm{IBR}}^{(4\cdots)}$, we have picked up the most important part of the contributions of double excitations, and by carrying out a complete third-order calculation we have included perturbatively a number of terms that would be missed by an all-orders method truncated at double excitations. While these contributions are small, they play a significant role at the level of precision considered here. They can be automatically picked up by all-orders methods involving triple excitations. However, because of their relative smallness, it does not seem worth the effort to implement these much more computationally demanding programs. It is our opinion that the approach most likely to lead to the next level of accuracy, the hundredth of a percent level, is the following. A complete all-orders method involving up to two excitations should be set up with high-quality numerical methods. In particular, as high a number of partial waves and as large a basis set as possible should be used. This will of necessity involve a large amount of computer time, which we estimate to be on the order of tens of hours of CRAY time. Any all-order method, as mentioned above, sums infinite classes of diagrams, but only a subset of the diagrams in any given order, as some diagrams will in general be associated with excitations of a higher order than used in the method. However, we have already in third order identified individual contributions, so that such terms can be added in to an all-orders method. The next step is to extend the calculation to fourth order. While a very large number of graphs are present in this order, a great number of them are automatically accounted for by the all-orders methods. We propose to evaluate the remaining graphs directly, in the same way that we calculated $E_A^{(4)}$. While we would expect these remaining graphs to be small, they will very likely contribute at the hundredth of a percent level, and should be included in the next stage of these precision calculations. One could even imagine extending this analysis to fifth order: however, at this level some automated scheme will certainly be necessary because of the enormous number of graphs present. The evaluation of the remaining fourth-order graphs is important for another reason. A very grave danger always present in the many-body problem comes from the fact that the perturbation expansion is complex, and contributions of relatively high order are significant. This makes it possible, in principle, to manipulate the calculation by simply including terms until agreement with experiment is found, and then stopping. For this reason it is vital to learn as much as possible about the perturbation expansion to ensure that one is not missing large terms that cancel for the property one is considering, but may not do so for a property one wishes to predict. The best way to do this is to carry out MBPT in an order-by-order manner.

One class of higher-order diagrams that has been stressed recently by Dzuba *et al.*[10] for thallium is the set of polarization or ring graphs. In third order these are represented by Figs. 1(a), 1(b), 1(g), and 1(h). We have not included the fourth- and higher-order ring graphs in this calculation. However, note that there is a strong cancellation in third order between the individually large contributions from Figs. 1(b) and 1(h). The good agreement found with experiment in this calculation is an indication that the higher-order polarization corrections are not as important for cesium as for thallium.

For the three states considered the Breit corrections to the energy are well below the level of numerical uncertainty quoted in Table I; we find these corrections to be 0.000 014 6, 0.000 034 2, and 0.000 004 9 a.u. for the $6s_{1/2}$, $6p_{1/2}$, and $7s_{1/2}$ states, respectively. It should be remarked that the relatively small size of these corrections is a result of random-phase-approximation (RPA) screening[8] which reduces the Breit correction to the $6s_{1/2}$ energy by an order of magnitude. The reduced mass and mass-polarization corrections are of order 1×10^{-7} a.u. and are therefore completely negligible at the present level of accuracy.

In conclusion, we have carried out a MBPT calculation complete through third order, including two types of higher-order corrections, for removal energies of valence states of cesium. Agreement with experiment at the few tenths of a percent level was found. The next stage of this investigation is to include infinite sets of diagrams associated with all-order methods based on double excitations, while calculating higher-order excitations perturbatively through fourth order. The principal reason for carrying out high-accuracy calculations on cesium is, however, for the prediction of PNC matrix elements. From our investigations we would conclude that the graphs considered here should be included at least as external legs in any matrix element calculation: this same procedure at second order is known to dramatically improve agreement between theory and experiment for parity-conserving matrix elements. Other kinds of graphs will also enter that are less directly related to the calculations of this paper. Once again, a direct implementation of MBPT through successively higher orders should allow for identification of the important graphs.

We would like to thank I. Lindgren, J. A. Pople, and O. Sushkov for several useful discussions. This work was supported in part by National Science Foundation (NSF) Grants No. PHY-85-0317 and No. PHY-86-08101. The calculations were carried out on the National Center for Supercomputing Applications CRAY XMP/48.

[1]M. C. Noecker, B. P. Masterson, and C. E. Wieman, Phys. Rev. Lett. **61**, 310 (1988).

[2]U. Amaldi *et al.*, Phys. Rev. D **36**, 1385 (1987).

[3]W. R. Johnson, M. Idrees, and J. Sapirstein, Phys. Rev. A **35**,

3218 (1987).
[4]W. R. Johnson, S. A. Blundell, Z. W. Liu, and J. Sapirstein, Phys. Rev. A **37**, 1395 (1988).
[5]I. Lindgren and J. Morrison, *Atomic Many-Body Theory,* 2nd ed. (Springer, Berlin, 1986).
[6]I. Lindgren, Phys. Rev. A **31**, 1273 (1985).
[7]I. Lindgren (private communcation).
[8]W. R. Johnson, S. A. Blundell, and J. Sapirstein, Phys. Rev. A **37**, 2764 (1988); **38**, 2699 (1988).
[9]We are indebted to Dr. J. A. Pople for this suggestion.
[10]V. A. Dzuba, V. V. Flambaum, P. G. Silvestrov, and O. P. Sushkov (unpublished).